Structural behaviour of reinforced concrete beams with self-healing cover zone as lost formwork

He, Shan; Nuri, Masi; Jonkers, Henk M.; Luković, Mladena; Schlangen, Erik

DOI
10.1016/j.dibe.2024.100458

Publication date
2024

Document Version
Final published version

Published in
Developments in the Built Environment

Developments in the Built Environment 18 (2024) 100458

Contents lists available at ScienceDirect

Developments in the Built Environment

journal homepage: www.sciencedirect.com/journal/developments-in-the-built-environment

Structural behaviour of reinforced concrete beams with self-healing cover zone as lost formwork

Shan He [a,*], Masi Nuri [b], Henk M. Jonkers [a], Mladena Luković [b], Erik Schlangen [a]

[a] Microlab, Faculty of Civil Engineering and Geosciences, Delft University of Technology, 2628, CN Delft, the Netherlands
[b] Concrete Structures, Faculty of Civil Engineering and Geosciences, Delft University of Technology, 2628, CN Delft, the Netherlands

ARTICLE INFO

Keywords:
SHCC
Self-healing
crack width control
Reinforced concrete beams

ABSTRACT

This study investigates the structural behaviour and self-healing performance of hybrid reinforced concrete (RC) beams, enhanced with a 1.5-cm-thick self-healing cover composed of bacteria-embedded strain hardening cementitious composite (SHCC), for its potential in crack width control and crack healing. The research focuses on the performance under both flexural and shear loading, examining aspects such as load-bearing capacity, surface crack pattern, crack propagation between layers, and healing effectiveness. Results demonstrate the successful activation of the healing function, alongside improvements in structural performance. Under flexural loading, hybrid beams exhibited greater load-bearing capacity and significantly improved crack control ability. The maximum crack width of the hybrid beams exceeded 0.3 mm at 124.7 kN load, whereas in the control beam the largest crack exceeded 0.3 mm at only 59.8 kN load. Under shear loading, while the influence of the cover on structural capacity was minimal, it notably improved post-peak ductility and energy dissipation. Interface delamination was not observed in both cases. The results of the current study demonstrate the potential of delivering the self-healing mechanism precisely where it is most needed, which presents a scalable and economically viable strategy for integrating self-healing technology into standard construction practices.

1. Introduction

Cracking in concrete is a common occurrence, as reinforced concrete structures are engineered to allow controlled cracking, enabling activation of the reinforcement. With appropriate reinforcement design, crack widths can be controlled and kept small, such that durability of a structure can be ensured throughout its intended service life. Consequently, infrastructures with extended service life requirements or exposure to aggressive environments often necessitate a considerable additional amount of reinforcement, in excess of what the structural capacity demands, and a thick cover to mitigate the likelihood of cracks exceeding acceptable widths. This often results in significant economic and environmental burdens as a result of inefficient use of materials.

Instead of designing extra reinforcement in excess of what the structural capacity demands, another strategy to 'manage' the risk of crack occurrence is to apply concrete with crack-healing capacity: self-healing concrete. Over the last decades, extensive research has been carried out either to stimulate the intrinsic/autogenous self-healing capacity of cementitious materials in general (*e.g.*, via the use of mineral additives (Huang et al., 2014; Yang et al., 2009a), crystalline admixtures (de Nardi et al., 2017; Ferrara et al., 2014), or superabsorbent polymers (Snoeck et al., 2012)), or to develop novel autonomous self-healing mechanisms (*e.g.*, via the application of micro- (Wang et al., 2014), macro- (Mullem et al., 2020), or vascular-encapsulated polymers (Shields et al., 2021), minerals, or bacteria (Jonkers et al., 2010)). Since the effectiveness of all healing approaches depend on the crack width, there is also a growing trend to explore the self-healing potential in materials with intrinsic crack width control ability. One of such materials is known as Strain Hardening Cementitious Composites (SHCC) (Li, 2019), which is a micro-fibre reinforced cement-based composite featuring high tensile ductility, enabled by the formation of multiple closely spaced micro-cracks that have an average crack width of only 60–80 μm (Li et al., 2002). Researchers have shown that SHCC, designed with mineral additives, can have increased autogenous self-healing capacity (Yang et al., 2009b; Qiu et al., 2016). Moreover, it was proved that the speed and extent of healing can be even more enhanced by embedding bacteria in SHCC (He et al., 2022a, 2023a).

Despite significant advancements in laboratory research, the use of self-healing concrete technologies in practical construction projects is still limited. This gap between research progress and real-world

* Corresponding author. Stevinweg 1, 2628, CN Delft, the Netherlands.
E-mail address: s.he-2@tudelft.nl (S. He).

https://doi.org/10.1016/j.dibe.2024.100458
Received 4 March 2024; Received in revised form 22 April 2024; Accepted 12 May 2024
Available online 13 May 2024

application can primarily be attributed to three factors, the first being the considerable costs involved in implementation. Self-healing concrete requires the incorporation of specialized components, such as bacterial spores or encapsulated healing agents, which substantially increase the material cost compared to traditional concrete ingredients like cement, sand, and gravel (Bandeira Barros et al., 2023; Silva et al., 2015). Although self-healing concrete promises long-term economic benefits through reduced maintenance needs and enhanced durability, accurately quantifying these advantages is challenging. Consequently, the immediate financial outlay often takes precedence in construction decision-making processes, where there is a marked preference for minimizing initial costs rather than investing in potential long-term savings. This necessitates the development of more cost-effective strategies for incorporating self-healing mechanisms into standard construction practices. The second factor is related to ensuring the efficacy of self-healing mechanisms when scaling up from laboratory experiments to full-scale concrete applications. Laboratory experiments typically focus on mortar specimens, which lack coarse aggregates present in concrete, thereby not fully simulating real-world conditions. When the proportion of healing agents, relative to the cement weight, remains unchanged in the transition from mortar to concrete, the inclusion of coarse aggregates dilutes the concentration of these agents. This dilution not only diminishes the healing capability but also decreases the probability of cracks intersecting the healing agents, thereby reducing the likelihood of activation. Such challenges underscore the need for optimizing the distribution and concentration of healing agents to preserve the self-healing efficiency when applied at structural levels. The third factor is the environmental impact of self-healing concretes. According to a recent study (Justo-Reinoso et al., 2023), bacteria-based self-healing concrete has an 85% higher environmental impact per cubic meter than conventional concrete due to the nutrients and calcium precursors needed by bacteria. Thus, the study suggests using bacteria-based self-healing concrete specifically in the cover zone of concrete structures to enable wider crack widths and decrease non-structural steel usage, thereby reducing the structure's carbon footprint.

Integrating the previously discussed challenges, a viable solution emerges in the form of a composite system, which includes a reinforced concrete core protected by a self-healing cover-zone. This approach, illustrated in Fig. 1, highlights the strategic application of self-healing techniques only at the cover-zone, which controls the overall durability of RC structures. This focused application in the cover-zone ensures that the self-healing mechanism is precisely where it is most needed for enhancing durability, thereby presenting a scalable and economically viable strategy for incorporating self-healing concrete into standard construction practices. In addition, previous studies on SHCC/RC hybrid elements have revealed superior cracking performance (He et al., 2023b; Mustafa et al., 2022), indicating conducive conditions for healing processes within these systems. However, it is noteworthy that the cracking behaviour hinges on the appropriate design of the interface between the layers.

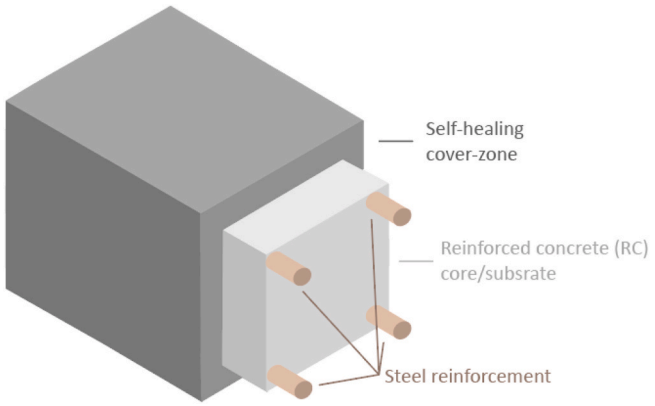

Fig. 1. Schematic illustration of RC beams with the self-healing cover zone.

The aim of the current study is to assess the structural response and self-healing effectiveness of reinforced concrete (RC) beams featuring a self-healing cover zone. This cover zone consists of a 15-mm-thick layer of cover made of self-healing strain-hardening cementitious composite (SH-SHCC), designed to control crack width and promote crack healing. The SH-SHCC contains bacteria-embedded polylactic acid (PLA) capsules and relies on bacteria-mediated calcium carbonate formation for crack healing. A total of 6 beams were prepared and tested, including 2 reference RC beams and 4 hybrid beams containing a 15-mm-thick U-shape SH-SHCC cover. These beams were divided into 2 groups for testing, one subjected to flexural loading and the other to shear loading. Digital image correlation (DIC) was employed for all the beams to monitor the deformation of the beams and the development of cracks. Interface openings between the cover and the core were also monitored with linear variable differential transformers (LVDTs). Subsequent to testing, the beams were cut into smaller segments. Certain segments underwent epoxy impregnation to investigate crack propagation from the core to the cover, while others underwent one month of moisture curing. Surface crack patterns before and after healing were then compared to qualitatively assess the healing performance.

2. Materials and tests

2.1. Experimental design

The testing protocol comprises two sets of beams: one exposed to flexural loading in a 4-point bending setup, and the other exposed to shear loading in a 3-point bending setup. In addition to investigating the load-deflection behaviour, each set of beams is tailored to address different testing objectives. For the beams subjected to flexural loading, the primary objective was to assess the potential of the SH-SHCC cover in enabling the development of fine cracks, thereby facilitating rapid healing. In the case of beams undergoing shear, emphasis is placed on evaluating the cracking behaviour and post-peak ductility.

Each set of beams contains 3 specimens, including 1 conventional reinforced concrete beam as a reference specimen and 2 hybrid beams consisting of a 15-mm-thick U-shape SH-SHCC cover as shown in Figs. 2 and 3. The reference beam in each set is denoted as Flex-R and Shear-R, and the reinforcement details were designed to ensure that they would fail in flexure and shear, respectively. The geometry and reinforcement details of the beams are given in Figs. 2 and 3. In both sets of beams, one stirrup was designed on each side outside the support region for easy handling of the beams. One hybrid beam in each set (Flex-1 and Shear-1) has a smooth interface between the bottom SH-SHCC layer and the reinforced concrete, while the other hybrid beam (Flex-2 and Shear-2) has a profiled interface which is made of a line of protruding shear-key from the SHCC layer. All interfaces between the cover and the core have been treated with a think layer of Vaseline to ensure their deformational compatibility. The shear-keys provide mechanical interlocking for structural integrity, while the Vaseline treatment allows controlled partial delamination between the SHCC and concrete layers, promoting deformation between the two layers. The design principles and geometric details of the pattern are discussed in our prior publication (He et al., 2023b). The pattern consists of equally sized and evenly spaced circular keys which have a diameter of 25 mm and a height of 10 mm. The spacing between the keys is 25 mm, which is designed such that the largest aggregate in the concrete can fill into the gap between 2 adjacent keys.

2.2. Materials and sample preparation

Table 1 shows the mixture compositions of SH-SHCC and concrete used in the current study. The mix design of the SHCC was developed in earlier research (He et al., 2022b). The self-healing performance of a

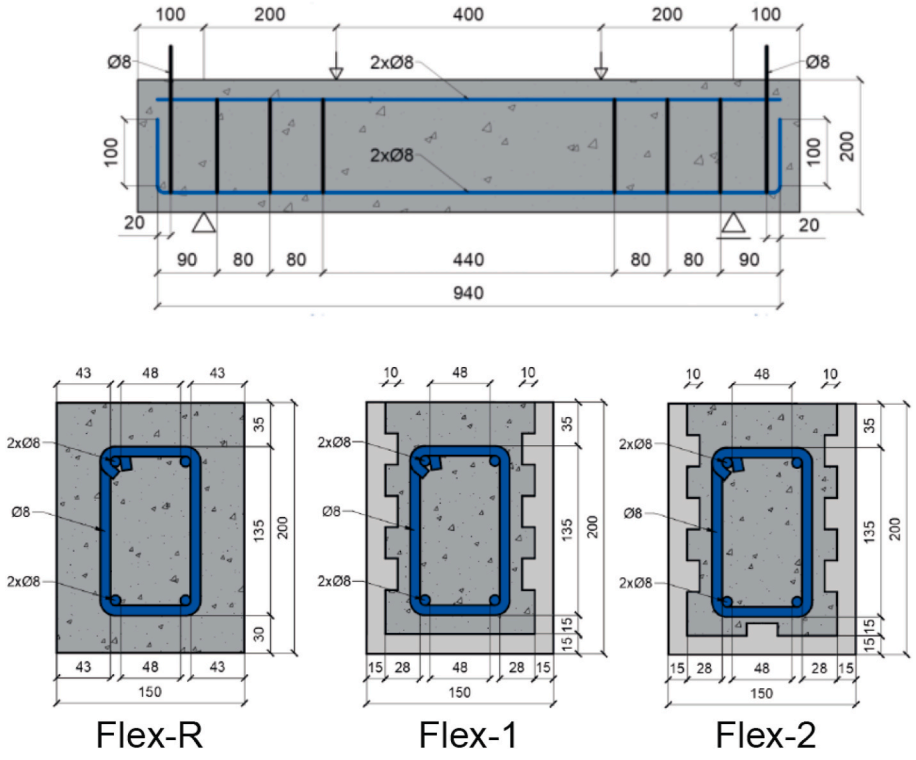

Fig. 2. Design details of the beams for 4-point-bending test [unit in mm].

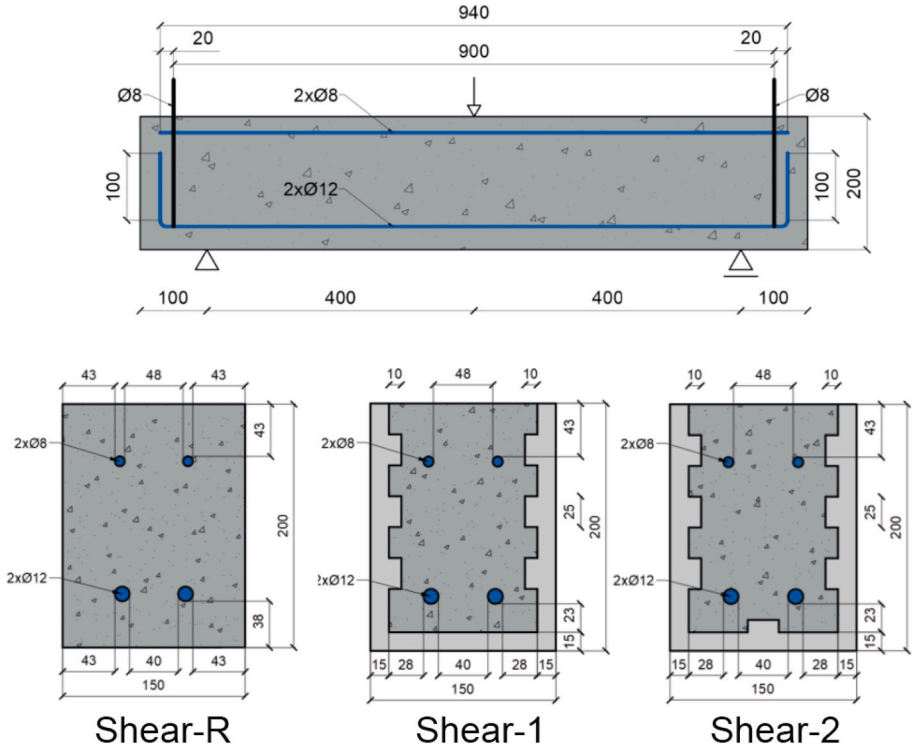

Fig. 3. Design details of the beams for 3-point-bending test [unit in mm].

comparable mix was also extensively assessed (He et al., 2023a). Specifically, the modified SH-SHCC matrix has a water-to-binder ratio of 0.4 and a filler-to-binder ratio of 0.5. Blast furnace slag (BFS) cement CEM III/B 42.5 N from ENCI (the Netherlands), consisting of 20–34 % clinker and 66–80% BFS, was used as binder and finely ground limestone powder Calcitec® from Carmeuse (Belgium) was used as filler. Silica fume was added to increase the bond strength between fibre and matrix (Chan and Li, 1997). A polycarboxylate-based superplasticizer (SP) MasterGlenium 51 produced from BASF (Germany) with 35.0% solid content by mass was used to reach desired workability. The fibre used in this study is ultra-high-molecular-weight polyethylene (UHMWPE) fibre with a length of 6 mm and diameter of 20 μm. Since the amount of fibre

Table 1
Mixture compositions of SH-SHCC and concrete [unit in kg/m3].

Material	SHCC	Concrete
CEM I 52.5 R	–	260
CEM III/B 42.5 N	842	–
Silica fume	94	–
Limestone powder	468	–
Sand (0.125–4 mm)	–	847
Gravel (4–16 mm)	–	1123
PE fiber (vol%)	10 (1%)	–
Healing agent	20	–
Water	374	156
Superplasticizer	3	0.26

has been addressed as the cause for workability, sustainability and cost, a separate study was carried by adjusting the mix design to reduce the amount of fibre from a typical 2%–1%. Owning to a thinner diameter and enhanced bonding due to the use of silica fume, the amount of fibre was reduced without sacrificing its tensile performance. Physical and mechanical properties of the fibre are presented in Table 2. The healing agent (HA) used is the self-healing bio-polymeric particles from Basilisk (the Netherlands). The HA is made of a poly-lactic acid (PLA) derivate matrix, bacterial spores of Bacillus cohnii-related strains and growth-required nutrient inorganic salts.

All the hybrid beams in the current study were casted in 2 steps. In the first step, SH-SHCC cover were cast inside a plywood mould against a piece of foam fixed at the bottom of the mould (Fig. 4). The foams were glued with 10-mm-thick silicon rubber sheets having a reverse shape of the desired shear-key pattern at both side walls. By casting the SH-SHCC into the remaining gap, the fresh material will fill into the holes of the rubber sheet and then form the resulting protruding keys as shown in Fig. 4. Subsequently, the materials were covered with plastic sheets and cured at room temperature for one day. The hardened specimens were then removed from the moulds and transferred to a climate-controlled room (20 °C and 98% RH) for an additional 14 days of curing. In the second step, SH-SHCC covers were taken out from the climate room and placed into plywood mould. On top of the SH-SHCC covers, reinforcement cages were placed with appropriate spacers. Subsequently, the concrete was cast and compacted using a vibration needle. The hybrid beams were then cured for 28 days in sealed conditions before testing.

To prepare the SH-SHCC materials, dry powders excluding healing agents were initially mixed using a Hobart® mixer for a duration of 5 min. Water, pre-mixed with 80% of SP, was gradually added to the mixture, continuously mixed until a uniform and consistent fresh paste was achieved. Following this, healing agents and fibres were gradually incorporated over a period of 5 min. Meanwhile, the remaining 20% SP was introduced to the mixture to offset any rheological changes resulting from fibre addition. The resulting fresh material was then cast into specialized moulds for the covers, as well as into polystyrene prism moulds (160 mm × 40 mm × 40 mm) and dog-bone moulds to determine compressive and tensile properties of the SH-SHCC material. To comply with recommendations from the Japan Society of Civil Engineers (JSCE) (Japan Society of Civil Engineers, 2008), dog-bone shaped specimens featuring a cross-section of 13 mm × 30 mm at the test zone were utilized. The geometry details of the dogbone and the testing setup has been reported in our previous publication (He et al., 2022a, 2023b). All casting operations were conducted on a vibration table to expel trapped air and enhance material filling into the holes in rubber sheet. the curing conditions for the dog-bones and prisms are the same as those of the SH-SHCC covers in the hybrid beams. The curing conditions for the dog-bones and prisms are the same as those of the SH-SHCC covers in the hybrid beams. Concrete cubes measuring 150 mm × 150 mm × 150 mm were also prepared following NEN-EN 12930-3 (Testing of hardened concrete, 2019) standards to determine the compressive strength of concrete.

Table 2
Physical and mechanical properties of PE fibers.

Length (mm)	Diameter (μm)	Density (kg/m3)	Nominal tensile strength (MPa)	Young's modulus (GPa)	Elongation at break
6	20	980	3000	110	3%

2.3. Testing

2.3.1. Structural tests of RC beams

The beams underwent testing in a four- or a three-point-bending configuration, as depicted in Fig. 5a. Both tests were conducted under displacement control of actuator at a rate of 0.01 mm/s, which relies on the feedback from an external displacement control (EDC). The relative vertical mid-point deflection of the beams with respect to the supports was measured using a LVDT while deformation of the beams was tracked using DIC on both sides. DIC is a method that analyses images captured during loading to monitor and record the surface movement of a deforming solid (Crammond et al., 2013; Pan et al., 2009). Prior to DIC measurement, specific regions of the beam were painted white and adorned with a black speckle pattern applied using an air gun. Images for DIC were captured at 10-s intervals throughout the loading process, with a resolution of 0.08 mm/pixel. Subsequently, post-processing of DIC results was performed using a freely available version of GOM Correlate software. Given that interfacial delamination typically poses a concern for layered systems, LVDTs were arranged atop the hybrid beams to detect the interfacial opening between the core and the cover. For beams subjected to 4-point bending, the measuring point is positioned at the mid-span, whereas for beams undergoing 3-point bending, two sets of LVDTs were installed 10 cm away from the loading point as shown in Fig. 5b.

2.3.2. Material property tests of SHCC and concrete

The compressive strength of the SH-SHCC was assessed following the guidelines for mortar, as outlined in NEN EN 196-1 (European committee for standardization, 2016). Cube specimens measuring 40 mm × 40 mm × 40 mm were cut from 40 mm × 40 mm × 160 mm prism specimens for this purpose. Uniaxial tension tests were conducted using a servo-hydraulic testing machine (Instron® 8872) with displacement control set at a rate of 0.005 mm/s. Prior to testing, the specimens were subjected to up to 0.2 MPa pre-stress after being positioned within a pair of tensile grips. Deformations were measured using two LVDTs with a gauge length of 80 mm. Tests ended when the applied tensile load decreased to less than 50% of the maximum load, at which point the load was released. The ultimate tensile strength (σ_{ult}) was determined as the maximum tensile stress experienced by the specimen during the experiment, while the tensile strain capacity (ε_{ult}) was defined as the strain value at which the load dropped to 90% of the ultimate value. A total of four samples were tested to ascertain the tensile properties of SH-SHCC, and the results are presented in Table 3.

2.4. Evaluation of healing performance

Given that the primary purpose of the U-shape cover is to facilitate self-healing, the healing effectiveness of the hybrid beams was evaluated. The self-healing performance was assessed by comparing surface crack patterns of a segment of the tested beam before and after a one-month healing period. This entailed examining beam segments before and after the healing period in a humid environment with a constant temperature of 20 °C. Photos of the cracked surface before and after healing were captured and digitally analysed.

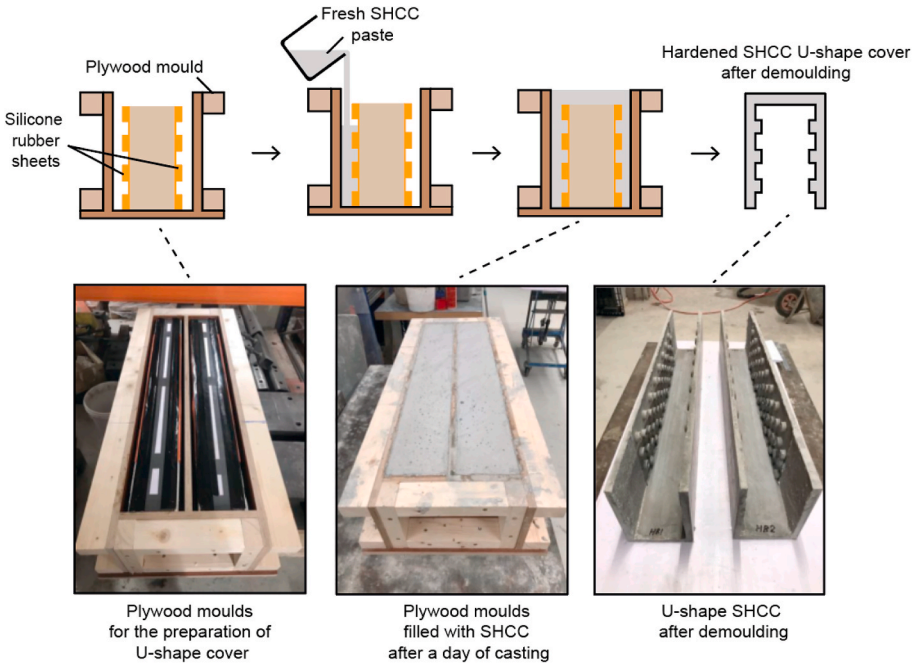

Fig. 4. Preparation procedure of the SH-SHCC cover.

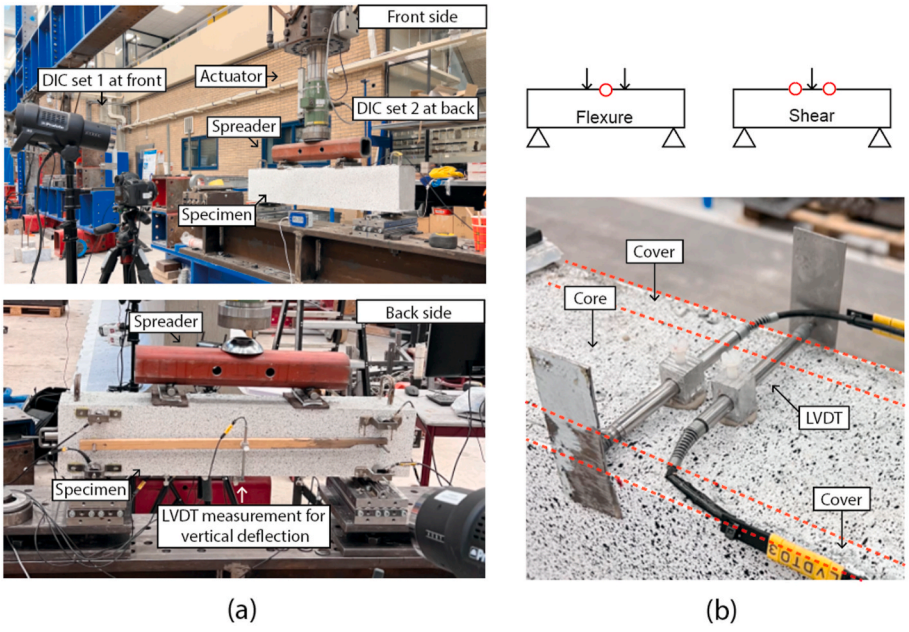

Fig. 5. (a) Experimental set-up for beam specimens with DIC measurement on both sides and (b) LVDT sets for the measurement of interfacial opening.

Table 3
Results of uniaxial compression and tension tests.

Mixture	Compressive strength (MPa)	First cracking strength (MPa)	Ultimate tensile strength (MPa)	Ultimate tensile strain (MPa)
SHCC	60.2 ± 0.7	1.9 ± 0.3	2.8 ± 0.26	2.6% ± 0.4%
Concrete	48.4 ± 2.0	–	–	–

3. Results and discussion

3.1. Material properties

Fig. 6 illustrates the typical stress-strain curves for SH-SHCC dog-bones. Notably, the mixture displayed significant tensile strain hardening behaviour with the emergence of multiple fine cracks, as depicted in Fig. 6. Furthermore, Table 3 provides a summary of the mechanical properties of SH-SHCC and concrete. SH-SHCC demonstrated an average tensile strain capacity of 2.6 % and an average tensile strength of 2.8 MPa. This combination of tensile properties ensured both the differential deformation between the cover and the core and the development of small cracks, which served to slow the penetration of aggressive ions

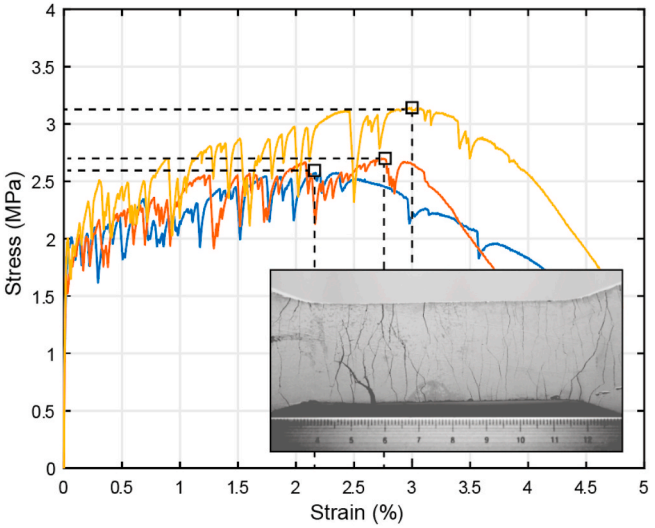

Fig. 6. Stress-strain curves of SH-SHCC under direction tension test.

while enabling swift and effective healing. In addition, the average compressive strengths of SH-SHCC and concrete were 60.2 MPa and 48.4 MPa, respectively. Opting for a relatively stronger SH-SHCC over traditional concrete was intended to ensure the cover's ability to withstand the stresses associated with demoulding, handling, and beam casting. This, in turn, opens up the possibility of utilizing the cover as lost formwork for the production of precast elements. Additionally, a stronger cover zone with a dense microstructure was anticipated to enhance the durability of the structural element.

3.2. Structural performance

3.2.1. Flexural behaviour

Fig. 7a illustrates the comparison of load versus mid-span deflection responses for the beams tested under flexural loads. It is evident that the load-deflection relationship of the hybrid beams (Flex-1 & Flex-2) differed significantly from that of the reference reinforced concrete beam (Flex-R). The hybrid beams exhibited a higher tension stiffening in the stabilized cracking stage, and a higher load-bearing capacity compared to the reference beam, although their deflection at peak load were slightly lower. While the reference beam reached a maximum load of 116.64 kN, the hybrid beams achieved 145.69 kN and 159.29 kN, respectively. Despite its modest 15 mm thickness, the tensile stresses of the SH-SHCC cover played a significant role in contributing to the bending moment resistance of the beam. The lower deflection at peak load observed in the hybrid beam can be attributed to a diminished rotation capacity. This is due to the SH-SHCC cover's ability to constrain the opening of non-dominant cracks in concrete, thereby restricting strain distribution in reinforcement and facilitating the localization of deformations in a single large crack. Similar behaviour has been noted in concrete beams strengthened by SHCC, ultra-high-performance concrete, and textile (He et al., 2023b; Schumacher, 2006; Oesterlee, 2010; Martinola et al., 2010).

Moreover, it is found that the interface properties between the cover and the core influenced the structural response of the entire beam. Fig. 7b illustrates the evolution of interface opening, measured by LVDTs on the top surface of the hybrid beams. Dotted lines represent readings from individual LVDTs, whereas solid lines depict the averaged results for each beam. Load-deflection curves are also presented within the same graph, facilitating the correlation between interface openings and applied loads. It is evident that the average opening values for both beams remained consistently below 0.1 mm throughout the tests. Despite concerns regarding interfacial delamination in layered systems, both hybrid beams exhibited robust structural integrity throughout the

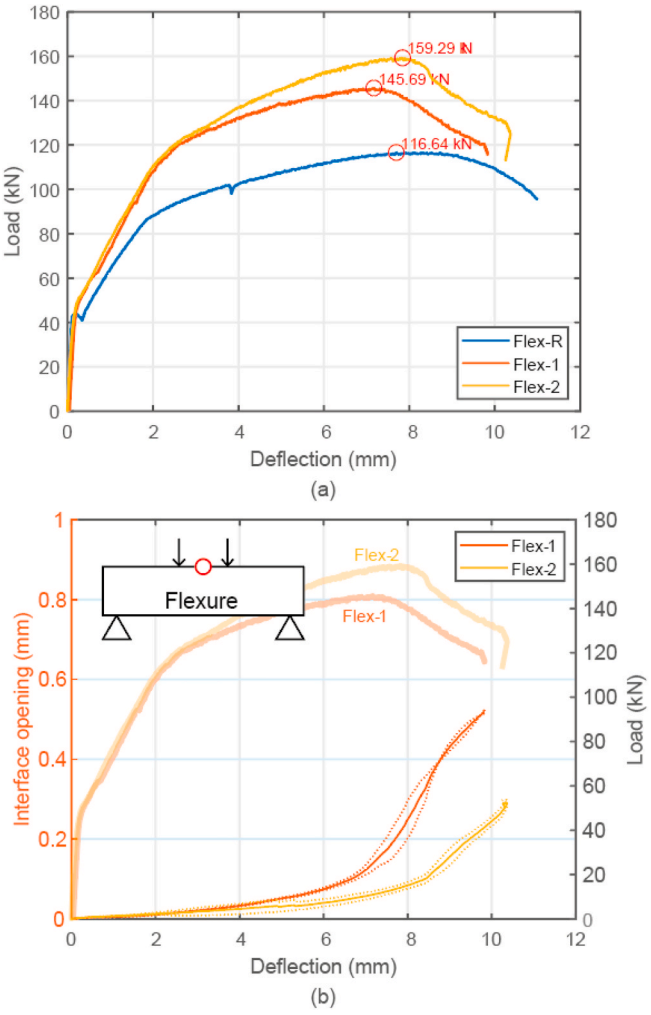

Fig. 7. (a) Load-deflection response of the tested beams under flexural loading and (b) interface opening between cover and core (each solid lines are averaged values from 2 LVDTs, while dotted lines are results from individual LVDTs). Load-deflection curves are also presented within the same graph, facilitating the correlation between interface openings and applied loads.

testing. Still, the presence of a line of shear-keys at the bottom interface provided additional mechanical resistance, resulting in a 14 kN increase in load-carrying capacity. This enhancement probably stems from a more synchronized behaviour between the cover and the core, leading to the activation of more SH-SHCC (both from the bottom and from the side) to bear the tensile load.

Fig. 8a depicts the crack patterns based on DIC principal strain analysis in the constant bending moment region for 4 key stages. These stages correspond to crack formation stage, stabilized cracking stage, reinforcement yielding stage, and ultimate stage of the reference beams. As can be seen, all beams failed as per design, exhibiting flexural tension failure characterized by flexural cracks on the tension side and concrete crushing on the compression side. The crack patterns reveal that the hybrid beams developed significantly more cracks compared to the reference beam. Unlike the reference beam, which exhibited only a few large cracks, the hybrid beams, equipped with the thin cover zones with microfibre reinforcement, displayed closely spaced fine cracks across the constant bending moment region. Additionally, the hybrid beam with bottom shear-key exhibited a higher number of cracks at all deflection levels, explaining its higher peak load capacity observed earlier.

All hybrid beams demonstrated enhanced control over crack widths. In Fig. 8b, the development of the maximum crack widths along the bottom edge of the beams, as a function of deflection, is depicted. The

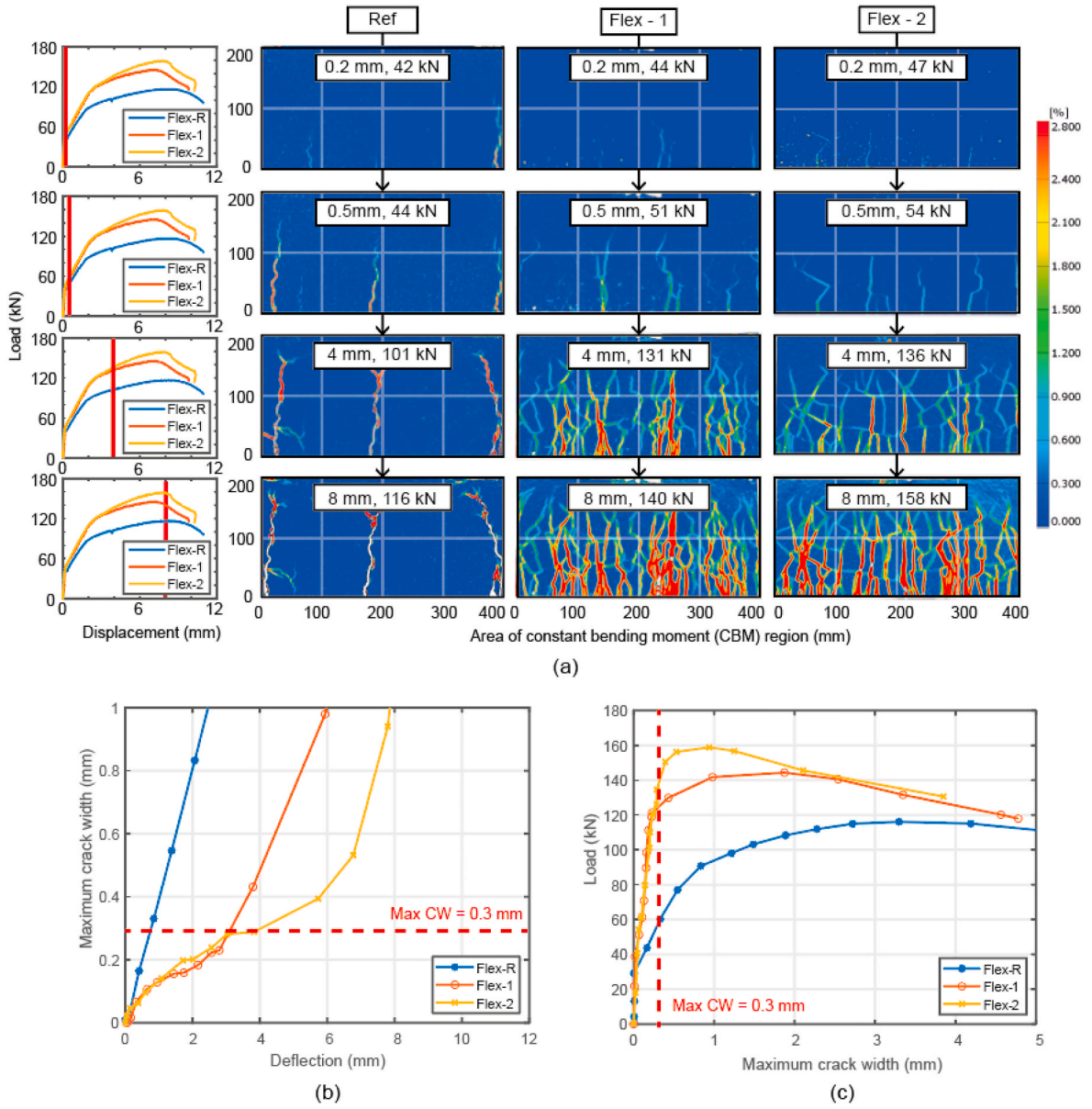

Fig. 8. (a) Crack pattern development at critical stages (i.e., crack initiation, reinforcement yielding and peak load), (b) development. of maximum crack width versus mid-point deflection, and (c) relation between load and maximum crack width.

maximum values correspond to the maximum crack width observed from the two side of beams by DIC. It is clear that the maximum crack width of the reference beam increased linearly with deflection. In contrast, for the hybrid beams, a distinct pattern of delayed crack width development was observed due to the generation of more cracks rather than the widening of existing ones. Consequently, the hybrid beams achieved higher load capacities while maintaining smaller crack widths (Fig. 8c). If a surface crack width limit of 0.3 mm is adopted as a benchmark, in line with the prescribed threshold in Eurocode 2 for reinforced concrete under quasi-permanent load across most exposure classes (excluding X0 and XC1), the reference beam exhibited maximum crack widths surpassing 0.3 mm at a load of 59.8 kN. Conversely, the hybrid beams managed to confine crack widths below 0.3 mm until reaching loads of 124.7 kN and 137.3 kN, respectively so after steel yielding.

Given that both load levels were achieved subsequent to reinforcement yielding, the quantity of reinforcement will be solely determined by the structural capacity necessary under the ultimate limit state. Therefore, no additional reinforcement will be required for the design pertaining to the service limit state. Moreover, this approach facilitates the efficient utilization of high-strength steel, where crack control consistently governs the design process.

3.2.2. *Shear behaviour*

Fig. 9a illustrates the load versus mid-span deflection curves for the beams subjected to shear loading. The purpose was to evaluate the reliability of the hybrid beams under shear. Shear-deficient beams without stirrups were thus made for the most critical situation where a very brittle failure is expected. Although all tested beams exhibited comparable peak loads, those with the SH-SHCC cover demonstrated higher stiffness after cracking and more ductile post-peak behaviour, marked by a gradual decrease in load. Post-cracking shear ductility refers to the ability of the beam to continue deforming and absorbing energy after the initiation of major shear crack under shear loading. It is an index to measure of the capacity of the beam to resist sudden shear failure and to sustain large deformations without collapsing (Qi et al., 2020). The post-cracking shear ductility of the beams can be expressed in terms of ductility factor (DF) as per Eq. (1). The DF has been defined

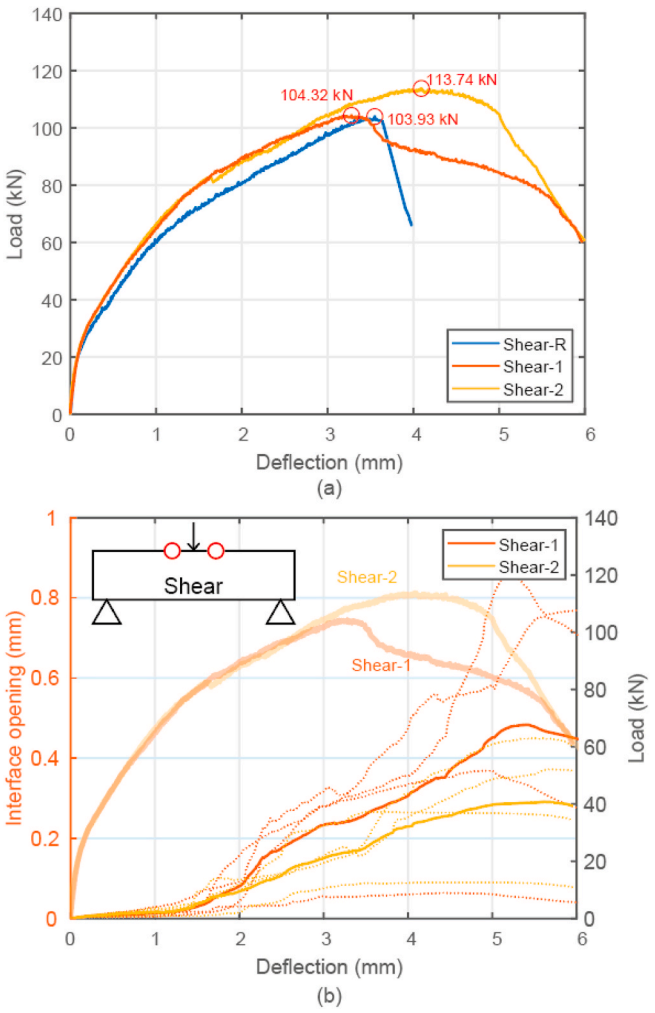

Fig. 9. (a) Load-deflection response of the tested beams under shear and (b) interface opening between cover and core (each solid lines are averaged values from 4 LVDTs, while dotted lines are results from individual LVDT). Load-deflection curves are also presented within the same graph, facilitating the correlation between interface openings and applied loads.

as the ratio of the deflection at failure load to the deflection at first diagonal crack load.

$$DF = \frac{\Delta_u}{\Delta_f} \tag{1}$$

In which Δ_u is the deflection at the peak load, Δ_f is the deflection at the initiation of major shear crack.

The DF values of the tested beams are summarized in Table 4. As can be seen, all hybrid beams exhibited higher DF than the reference beam. In RC members, the shear resistance of concrete elements depends on aggregate interlock mechanism, dowel action of the reinforcement, and uncracked compression zone. When SH-SHCC is applied on the lateral surface of the beams, the fibre bridging stresses in the SH-SHCC can be considered as an additional source of post-cracking shear resistance and thus contributed to an enhanced DF value.

Energy absorption capacities of all tested beams are also provided in Table 4. Energy absorption was calculated by measuring the area under the load-deflection curves until the load drops to 85% of the peak load. The two hybrid beams exhibited roughly 27% and 100% higher energy absorption capacities than the reference beam, respectively. The increase of energy absorption of hybrid beams was achieved due to higher deformation capacity and strain hardening characteristics of SH-SHCC. In addition, it was noticed that the shear key pattern at the bottom led to higher energy absorption increase.

Crucially, the experiment revealed no delamination between the cover and the core. This is evidenced by Fig. 9b, where the measured interface opening from four locations near the loading point remained consistently below 1 mm throughout the test duration. Despite slight variability in individual measurements, the average values consistently stayed below 0.3 mm before reaching peak load. Similarly as observed in flexural tests, higher capacity was observed in sample with the shear key pattern on the bottom, in which also crack opening at the interface stayed smaller throughout the test (Shear-2).

To capture the damage process of the beams, the evolution of crack pattern within the effective span at 3 critical moments (*i.e.*, the formation of the first flexural crack, the initiation of major shear crack, and the ultimate state) for all the tested beams are exported based on DIC principal strain analysis and are shown in Fig. 10. The representative cracking moments are also indicated in the load-deflection curves by the vertical red lines. As can be seen, the crack patterns of the hybrid beams were largely different than the reference beam. Instead of forming sparsely spaced diagonal shear cracks, the hybrid beams with SHCC cover exhibited a unique crack pattern, which is characterized by the formation of bundles of fine cracks. It is possible that the dominate shear cracks formed in conventional concrete core were arrested by the SHCC layer and turned into multiple fine cracks in the SHCC. Although the capacity was not significantly affected (by 9.5% in increased in Shear-2 beam), the hybrid beams can still benefit from the increased post-peak ductility conveyed by the formation of multiple micro-cracks.

3.3. Crack propagation

To further investigate the impact of the SH-SHCC cover in enabling the monolithic response in the hybrid structure and enhancing micro-cracking formation, the tested beams were sawn into smaller sections (Fig. 11a), which were subsequently epoxy impregnated for visualizing the crack path. From the cross-section of the beams (Fig. 11b), the cover and the core can be distinguished: due to the high slag content in the SH-SHCC, the cover area appeared to be blueish/greenish. Furthermore, it is evident that concrete has densely filled the space between the shear keys, showcasing the successful implementation of the concept.

To visualize how cracks propagate from the core to the cover, a corner piece was further cut out from the section. As can be seen from Fig. 11c, a major crack in the concrete core was successfully arrested and spread into multiple fine cracks both on the front and bottom sides of the cover. It's important to note that cracks did not necessarily need to form in the concrete first in order to activate the SHCC layer. It can be that the bottom SH-SHCC, where tensile stresses are greatest, cracks first, which then initiates a crack in the concrete core. What's crucial is that the multiple cracking behaviour of SH-SHCC ensures that a single large crack in concrete doesn't propagate into an equally wide crack in the SH-

Table 4
Summary of structural responses of tested beams under shear.

Beam ID	Flexural crack formation		Major shear crack initiation		Ultimate point		Ductility factor	Energy absorption (kN·mm)
	Load (kN)	Deflection (mm)	Load (kN)	Deflection (mm)	Load (kN)	Deflection (mm)		
Shear-R	16.0	0.21	38.9	0.44	103.7	3.55	8.54	530.8
Shear-1	17.5	0.22	40.2	0.40	103.7	3.28	11.0	672.5
Shear-2	20.2	0.21	43.7	0.46	113.5	4.09	11.2	1096.2

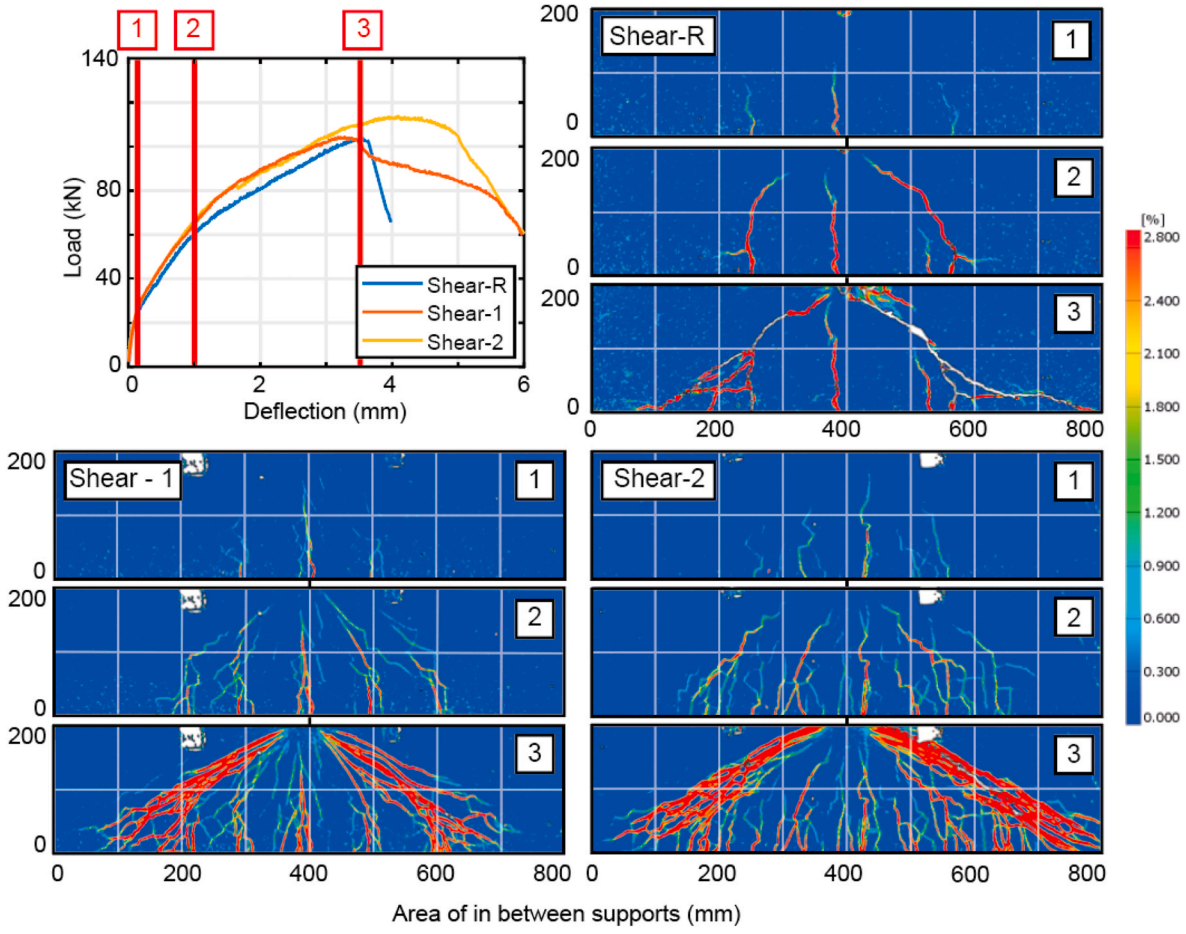

Fig. 10. Crack pattern development at critical stages (i.e., flexural crack initiation, shear crack initiation and peak load).

SHCC, thereby arresting the crack propagation.

Upon closer examination of the cross-section depicting the crack path toward the bottom surface (Fig. 11d), it is evident that the entire section of the SH-SHCC cover is engaged, with evenly distributed fine cracks forming beneath the primary crack in the concrete. By spreading the centralized deformation to the whole section, not only healing can happen must easier and faster, but the effective crack width that governs the speed of ion diffusion from the outer environment to the rebar is significantly reduced. This concept is presented schematically in Fig. 12a. It has been demonstrated by many that cracks represent spatial discontinuities in which the transport of moisture and chlorides is significant and that the effect of cracking on durability is significantly dependent on the crack width (Gérard and Marchand, 2000; Ismail et al., 2008; Jacobsen et al., 1996). Therefore, even if the cover did not have a healing ability, only the reduction of effective crack width can increase the durability of the structural elements. It is also important to emphasize that assessing the effective crack width in hybrid structures becomes challenging. Interfaces introduce non-linear deformation that can redirect cracks into configurations where propagation becomes more challenging. As depicted in Fig. 12b and c, the ultimate failure crack in concrete was diverted within the cover, yet connected by a fine interfacial crack between the cover and the core. The impact of interface opening on moisture and chloride ingress remains unclear.

3.4. Healing performance

Fig. 13 presents a comparative analysis of the bottom surface of a beam segment before and after the healing process. Binary images, highlighting the crack patterns, accompany the original photos. To ensure fairness in comparison, identical thresholds were applied to generate the binary images. As can be seen, the results reveal obvious healing of most cracks after a one-month period, indicating the effectiveness of the self-healing mechanism. However, it is evident that not all cracks fully healed within this timeframe. Larger cracks may require more time for complete recovery. Also, the random distribution of healing agents within the matrix may result in certain areas of cracks lacking sufficient agents to facilitate healing. Consequently, healing in these regions relies on autogenous healing of SHCC and bacterial migration from other parts of the cracks, leading to prolonged healing durations. Nevertheless, since the diffusion rate of most ions depends on the crack width (Yoon and Schlangen, 2014), even partially healed cracks are expected to contribute to an increase of durability.

It is important to emphasize that the healing agents utilized in this study are commercial products with a tailored particle size of approximately 1 mm. This design is specifically crafted to facilitate the healing of relatively large cracks commonly encountered in reinforced concrete structures. Notably, when employing the SH-SHCC cover, as shown in this study, smaller crack widths at similar loads can be expected. Therefore, adjustments in the particle size of the healing agents could be made accordingly. Decreasing the particle size of the healing agents would result in a higher number of particles per unit volume of concrete at the same dosage. Consequently, this increases the likelihood of cracks intersecting with healing agents, enhancing the overall healing efficacy.

In summary, our study demonstrates the successful activation of the healing function, alongside improvements in structural performance such as cracking behaviour, load-bearing capacity, and ductility. This challenges the previous perception that incorporating healing might inevitably compromise concrete's mechanical properties. Through

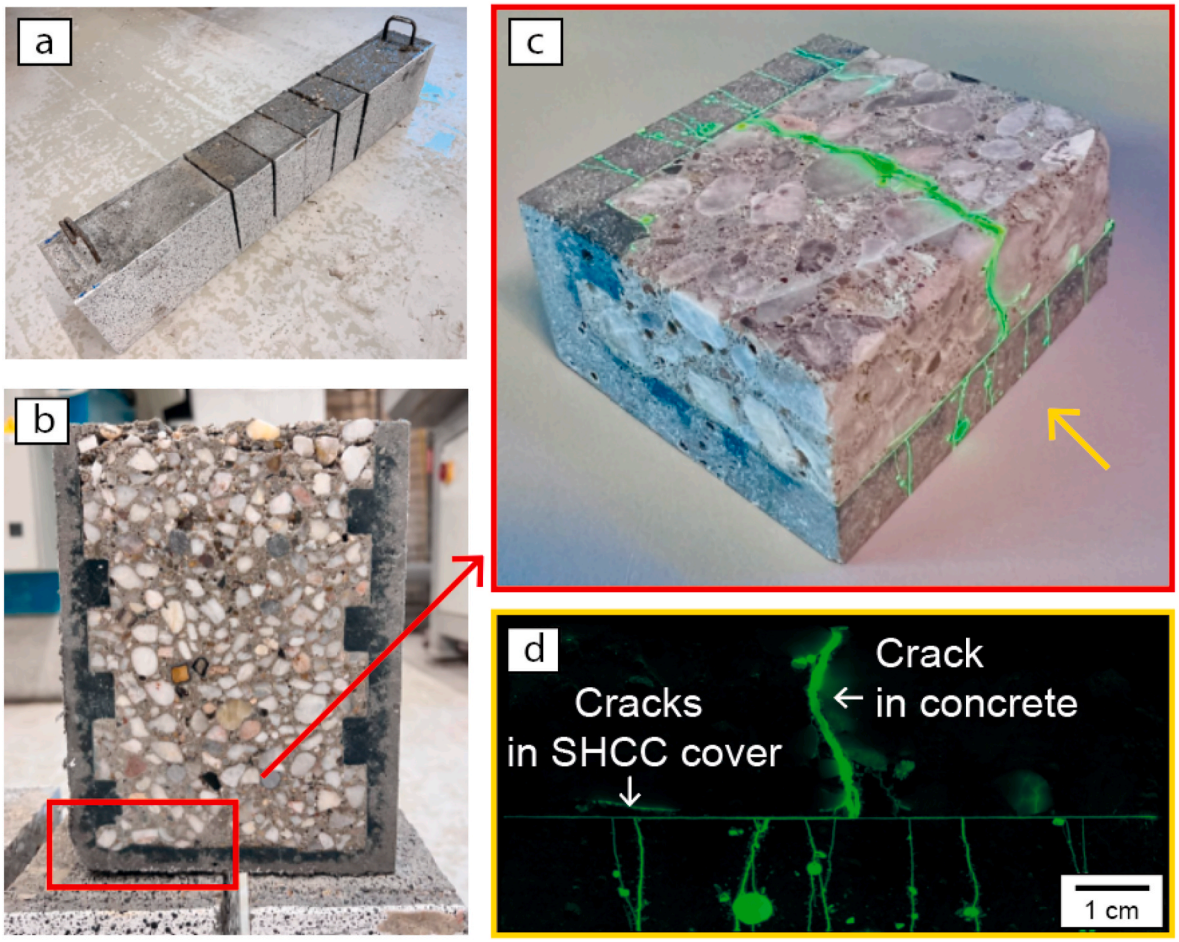

Fig. 11. (a) Tested beams after sawing (beam length: 1 m), (b) cross-sectional image of a section demonstrating the covered system, (c) corner piece cut from the beam section after epoxy impregnation, (d) front surface of the corner specimen under UV light to highlight the crack path.

strategic deployment of the self-healing mechanism, our research presents a scalable and economically viable strategy for integrating self-healing concrete into standard construction practices.

4. Conclusions

An experimental study was performed aiming to investigate the structural and healing behaviour of hybrid reinforced concrete beams with a self-healing cover made with bacteria embedded SHCC. Structural behaviour, surface crack pattern, and crack propagation between the reinforced concrete core and U-shaped SH-SHCC cover were studied. A qualitative assessment of the crack appearance before and after healing was also presented. The main findings of the current study are.

1. Under flexural loading, hybrid beams with the cover exhibited an enhanced crack control capability and higher load-bearing capacity (up to 35% greater) compared to the control beam. The maximum crack width of the best performing hybrid beams exceeded 0.3 mm at approximately 137 kN, whereas in the control beam, it exceeded 0.3 mm at only 63 kN load. The reduced crack width is expected to largely facilitate crack healing in the cover zone.
2. Under shear loading, the cover had minimal effect on structural capacity but affected cracking behaviour. It also enhanced post-peak ductility and energy dissipation capacity. In addition to the flexural cracks, the cover has been demonstrated to effectively distribute rapidly formed shear cracks into multiple fine cracks.
3. Delamination between the cover and core was not observed under both flexural and shear failure modes, a result attributed to the deformational capacity of the SH-SHCC and the tailored interface profile, specifically the shear-key pattern.
4. Characterization of the crack path from the concrete core to the cover confirms that the SH-SHCC cover can not only effectively spread a major crack in concrete into multiple fine cracks within the SHCC but to also block the main transport path by diverting the crack paths. This distribution of a major crack into multiple fine ones enhances the likelihood of the crack plane intersecting with the healing agent, while simultaneously decreasing the average crack width, thus facilitating easier healing.
5. Evident crack healing was observed after a period of 1-month moist curing. Despite that not all cracks had fully closed within this timeframe, those that remained were visibly shorter and smaller, indicating a positive progression of healing. While the current study primarily examined the structural behaviour and visually assessed the performance of healing, future studies are encouraged to explore the influence of healing on durability-related indicators of hybrid RC elements, such as the chloride ingress or carbonation induced corrosion.

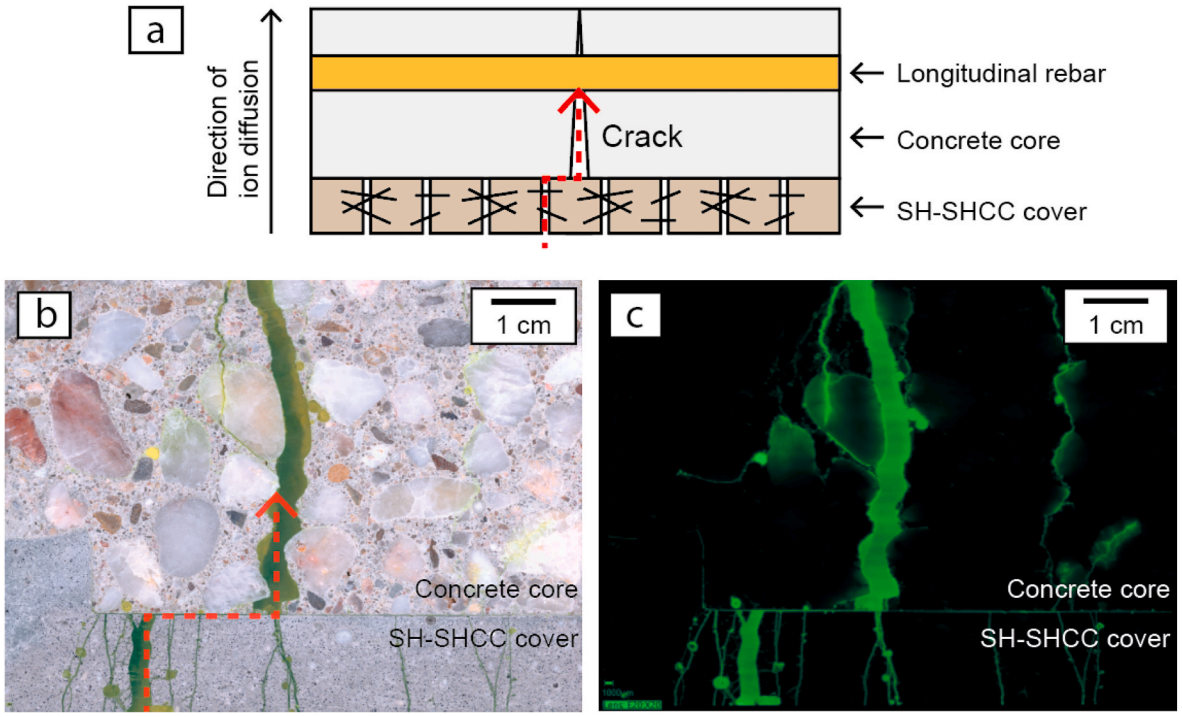

Fig. 12. (a) Schematic illustration depicting how SHCC cover obstructs the pathway for external ions to reach the rebar, (b) optical microscope image of an epoxy impregnated specimen sawn from tested beams, and (c) the same specimen under UV light for highlighting the crack path.

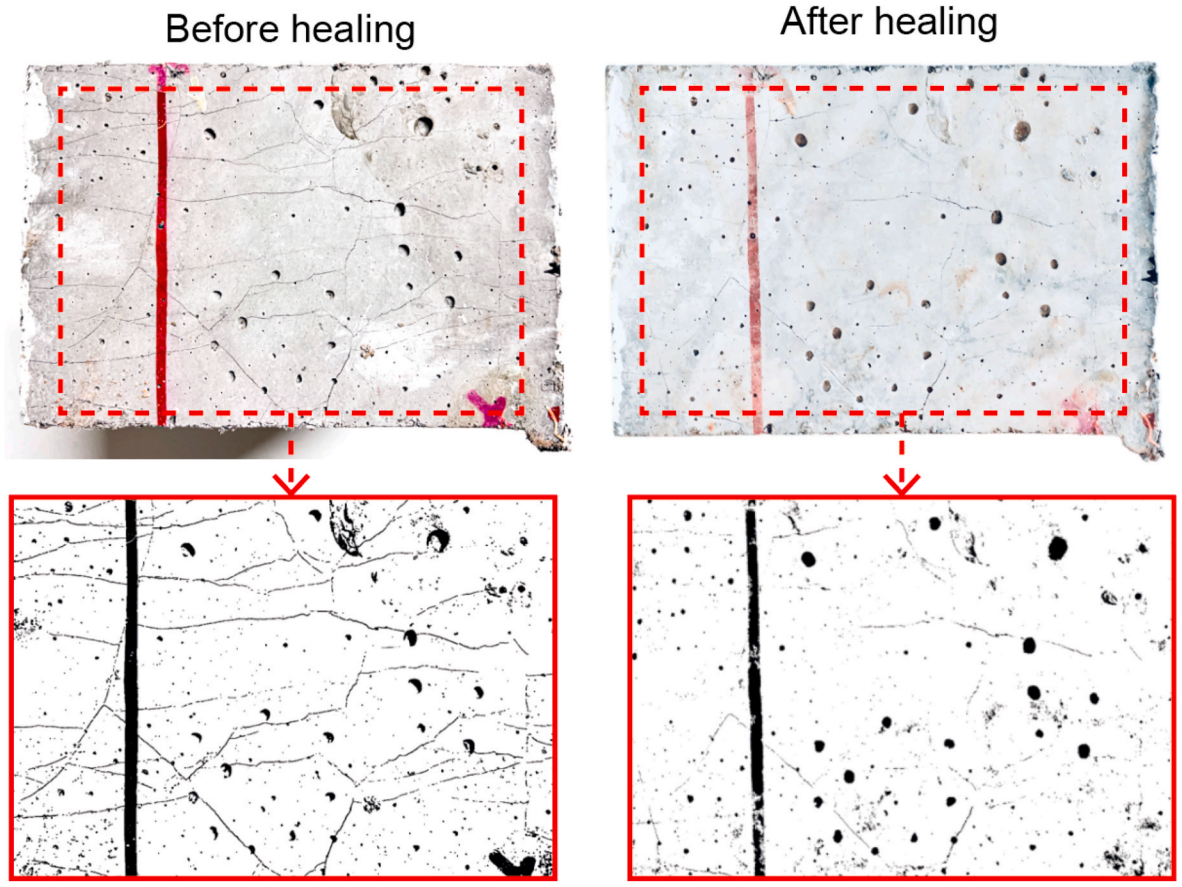

Fig. 13. Visual comparison of crack patterns on the bottom surface of tested beams before and after healing.

CRediT authorship contribution statement

Shan He: Writing – review & editing, Writing – original draft, Visualization, Validation, Methodology, Investigation, Formal analysis, Data curation. **Masi Nuri:** Visualization, Validation, Investigation, Data curation. **Henk M. Jonkers:** Supervision, Resources, Project administration, Funding acquisition. **Mladena Luković:** Supervision, Software, Resources, Project administration, Methodology, Funding acquisition, Conceptualization. **Erik Schlangen:** Supervision, Resources, Project administration, Funding acquisition, Conceptualization.

Declaration of competing interest

The authors declare that they have no known competing financial interests or personal relationships that could have appeared to influence the work reported in this paper.

Data availability

Data will be made available on request.

Acknowledgement

The authors acknowledge the financial supports from the MSCA-ITN project SMARTINCS. This project has received funding from the European Union's Horizon 2020 research and innovation programme under the Marie Skłodowska-Curie grant agreement No 860006.

References

Bandeira Barros, L., Knockaert, M., Tenório, R., 2023. An analysis of the commercialisation barriers of self-healing concrete. MATEC Web Conf 378.

Chan, Y.W., Li, V.C., 1997. Effects of transition zone densification on fiber/cement paste bond strength improvement. Adv. Cement Base Mater. 5, 8–17. https://doi.org/10.1016/S1065-7355(97)90010-9.

Crammond, G., Boyd, S.W., Dulieu-Barton, J.M., 2013. Speckle pattern quality assessment for digital image correlation. Opt Lasers Eng 51, 1368–1378. https://doi.org/10.1016/J.OPTLASENG.2013.03.014.

de Nardi, C., Bullo, S., Ferrara, L., Ronchin, L., Vavasori, A., 2017. Effectiveness of crystalline admixtures and lime/cement coated granules in engineered self-healing capacity of lime mortars. Mater. Struct. 50 (50), 1–12. https://doi.org/10.1617/S11527-017-1053-3, 4 2017.

European committee for standardization, 2016. NEN-EN 196-1. Methods of Testing Cement - Part 1. Determination of strength.

Ferrara, L., Krelani, V., Carsana, M., 2014. A "fracture testing" based approach to assess crack healing of concrete with and without crystalline admixtures. Constr Build Mater 68, 535–551. https://doi.org/10.1016/J.CONBUILDMAT.2014.07.008.

Gérard, B., Marchand, J., 2000. Influence of Cracking on the Diffusion Properties of Cement-Based Materials Part I: Influence of Continuous Cracks on the Steady-State Regime, vol. 30.

He, S., Zhang, S., Luković, M., Schlangen, E., 2022a. Effects of bacteria-embedded polylactic acid (PLA) capsules on fracture properties of strain hardening cementitious composite (SHCC). Eng. Fract. Mech. 268, 108480.

He, S., Zhang, S., Luković, M., Schlangen, E., 2022b. Effects of bacteria-embedded polylactic acid (PLA) capsules on fracture properties of strain hardening cementitious composite (SHCC). Eng. Fract. Mech. 268, 108480 https://doi.org/10.1016/J.ENGFRACMECH.2022.108480.

He, S., Wan, Z., Chen, Y., Jonkers, H.M., Schlangen, E., 2023a. Microstructural characterization of crack-healing enabled by bacteria-embedded polylactic acid (PLA) capsules. Cem. Concr. Compos. 143 https://doi.org/10.1016/j.cemconcomp.2023.105271.

He, S., Mustafa, S., Chang, Z., Liang, M., Schlangen, E., Luković, M., 2023b. Ultra-thin Strain Hardening Cementitious Composite (SHCC) layer in reinforced concrete cover zone for crack width control. Eng. Struct. 292, 116584.

Huang, H., Ye, G., Damidot, D., 2014. Effect of blast furnace slag on self-healing of microcracks in cementitious materials. Cem Concr Res 60, 68–82. https://doi.org/10.1016/J.CEMCONRES.2014.03.010.

Ismail, M., Toumi, A., François, R., Gagné, R., 2008. Effect of crack opening on the local diffusion of chloride in cracked mortar samples. Cem Concr Res 38, 1106–1111. https://doi.org/10.1016/j.cemconres.2008.03.009.

Jacobsen, S., Marchand, J., Boisvert, L., 1996. Effect of cracking and healing on chloride transport in OPC concrete. Cem Concr Res 26, 869–881. https://doi.org/10.1016/0008-8846(96)00072-5.

Japan Society of Civil Engineers, 2008. Recommendations for Design and Construction of High Performance Fiber Reinforced Cement Composites with Multiple Fine Cracks (HPFRCC).

Jonkers, H.M., Thijssen, A., Muyzer, G., Copuroglu, O., Schlangen, E., 2010. Application of bacteria as self-healing agent for the development of sustainable concrete. Ecol. Eng. 36, 230–235. https://doi.org/10.1016/J.ECOLENG.2008.12.036.

Justo-Reinoso, I., Arena, N., Reeksting, B.J., Gebhard, S., Paine, K., 2023. Bacteria-based self-healing concrete– A life cycle assessment perspective. Developments in the Built Environment 16, 100244. https://doi.org/10.1016/J.DIBE.2023.100244.

Li, V.C., 2019. Engineered cementitious composites (ECC). Engineered Cementitious Composites (ECC). https://doi.org/10.1007/978-3-662-58438-5.

Li, V.C., Wu, C., Wang, S., Ogawa, A., Saito, T., 2002. Interface tailoring for strain-hardening Polyvinyl Alcohol-engineered cementitious composite (PVA-ECC). Materials Journal 99, 463–472. https://doi.org/10.14359/12325.

Martinola, G., Meda, A., Plizzari, G.A., Rinaldi, Z., 2010. Strengthening and repair of RC beams with fiber reinforced concrete. Cem. Concr. Compos. 32, 731–739. https://doi.org/10.1016/J.CEMCONCOMP.2010.07.001.

Mullem, T Van, Anglani, G., Dudek, M., Vanoutrive, H., Bumanis, G., Litina, C., et al., 2020. Addressing the need for standardization of test methods for self-healing concrete: an inter-laboratory study on concrete with macrocapsules. Sci. Technol. Adv. Mater. 21, 661–682. https://doi.org/10.1080/14686996.2020.1814117.

Mustafa, S., Singh, S., Hordijk, D., Schlangen, E., Luković, M., 2022. Experimental and numerical investigation on the role of interface for crack-width control of hybrid SHCC concrete beams. Eng. Struct. 251, 113378 https://doi.org/10.1016/J.ENGSTRUCT.2021.113378.

Oesterlee, C., 2010. Structural Response of Reinforced UHPFRC and RC Composite Members. https://doi.org/10.5075/EPFL-THESIS-4848.

Pan, B., Qian, K., Xie, H., Asundi, A., 2009. Two-dimensional digital image correlation for in-plane displacement and strain measurement: a review. Meas. Sci. Technol. 20 https://doi.org/10.1088/0957-0233/20/6/062001.

Qi, J., Ma, Z.J., Wang, J., Bao, Y., 2020. Post-cracking shear behaviour of concrete beams strengthened with externally prestressed tendons. Structures 23, 214–224. https://doi.org/10.1016/J.ISTRUC.2019.09.009.

Qiu, J., Tan, H.S., Yang, E.H., 2016. Coupled effects of crack width, slag content, and conditioning alkalinity on autogenous healing of engineered cementitious composites. Cem. Concr. Compos. 73, 203–212. https://doi.org/10.1016/J.CEMCONCOMP.2016.07.013.

Schumacher, P., 2006. Rotation Capacity of Self-Compacting Steel Fiber Reinforced Concrete.

Shields, Y., Belie, N de, Jefferson, A., Tittelboom, K van, 2021. A review of vascular networks for self-healing applications. Smart Mater. Struct. 30, 063001 https://doi.org/10.1088/1361-665X/ABF41D.

Silva, F.B., Boon, N., De Belie, N., Verstraete, W., 2015. Industrial application of biological self-healing concrete: challenges and economical feasibility. J Commer Biotechnol 21, 31–38. https://doi.org/10.5912/JCB662.

Snoeck, D., Van Tittelboom, K., Steuperaert, S., Dubruel, P., De Belie, N., 2012. Self-healing cementitious materials by the combination of microfibres and superabsorbent polymers. J. Intell. Mater. Syst. Struct. 25, 13–24. https://doi.org/10.1177/1045389X12438623.

Testing of Hardened Concrete - Part 3: Compressive Strength of Test Pieces. NEN-EN 12930-3. Testing of Hardened Concrete - Part 3: Compressive Strength of Test Pieces, 2019.

Wang, J.Y., Soens, H., Verstraete, W., de Belie, N., 2014. Self-healing concrete by use of microencapsulated bacterial spores. Cem Concr Res 56, 139–152. https://doi.org/10.1016/J.CEMCONRES.2013.11.009.

Yang, Y., Lepech, M.D., Yang, E.H., Li, V.C., 2009a. Autogenous healing of engineered cementitious composites under wet–dry cycles. Cem Concr Res 39, 382–390. https://doi.org/10.1016/J.CEMCONRES.2009.01.013.

Yang, Y., Lepech, M.D., Yang, E.H., Li, V.C., 2009b. Autogenous healing of engineered cementitious composites under wet–dry cycles. Cem Concr Res 39, 382–390. https://doi.org/10.1016/J.CEMCONRES.2009.01.013.

Yoon, I.S., Schlangen, E., 2014. Experimental examination on chloride penetration through micro-crack in concrete. KSCE J. Civ. Eng. 18, 188–198. https://doi.org/10.1007/s12205-014-0196-9.